PNAS RESEARCH ARTICLE | GENETICS

Tai/NCOA2 suppresses the Hedgehog pathway by directly targeting the transcription factor Ci/GLI

Xuan Yu[a], Xinyu Wang[a], Kaize Ma[a], Dongqing Gao[a], Yanran Deng[b], Dafa Zhou[a], Wenhao Ding[a], Yunhe Zhao[a], Qingxin Liu[a], and Zizhang Zhou[a,b,1]

Affiliations are included on p. 11.

Edited by Natalia A. Riobo-Del Galdo, University of Leeds, Leeds, United Kingdom; received May 12, 2024; accepted October 10, 2024 by Editorial Board Member Matthew P. Scott

The Hedgehog (Hh) pathway plays diverse roles in cellular processes by activating the transcription factor Cubitus interruptus (Ci). Abnormal regulation of this pathway has been linked to various human diseases. While previous studies have focused on how Ci is regulated in the cytoplasm, the control of nuclear Ci remains poorly understood. In this study, we have found that the transcriptional cofactor Taiman (Tai) functions as an inhibitor of the Hh pathway. Tai interferes with the response of Hh signal, rather than Hh secretion. Our epistatic analyses reveal that Tai works in parallel with Ci to reduce its activity, thereby counteracting organ overgrowth and the activation of target genes caused by Ci overexpression. Specifically, Tai interacts with Ci to decrease its binding to target gene promoters. The Hh signal weakens the interaction between Ci and Tai, releasing the inhibition on Ci. Importantly, this regulatory mechanism is conserved from *Drosophila* to mammalian cells. Moreover, NCOA1-3 are the mammalian ortholog of *Drosophila* protein Tai, but only NCOA2 plays a similar role in inhibiting the Hh pathway. These findings reveal an additional way to modulate the transcriptional activity of nuclear Ci.

Hh pathway | Ci | Tai | LxxLL motif | NCOA2

Significance

The Hedgehog (Hh) pathway is crucial for organ development and pattern formation. At the core of this pathway is the transcription factor Cubitus interruptus (Ci). However, the regulation of nuclear Ci is not well understood. In this study, we have identified that Taiman (Tai) as a steroid-receptor coactivator, also negatively regulates the Hh pathway. Mechanistically, Tai interacts with the DNA-binding domain of Ci via its Leucine-x-x-Leucine-Leucine (LxxLL) motifs, which hinders Ci's ability to bind to DNA. The mammalian ortholog of Tai, nuclear receptor coactivator 2 (NCOA2), plays a similar role in inhibiting the Hh pathway. These findings uncover a mechanism for controlling the activation of nuclear Ci and highlight NCOA2 as a potential therapeutic target for Hh-responsive cancers.

The evolutionarily conserved Hedgehog (Hh) pathway plays crucial roles in pattern formation and organogenesis across species (1, 2). Disruption of Hh signaling leads to developmental abnormalities and cancer (3). The *Drosophila* wing disc serves as a valuable model for studying the Hh pathway. In the wing disc, Hh protein is produced in the posterior (P) compartment and diffuses into the anterior (A) compartment, creating a gradient (4, 5). The transcription factor Cubitus interruptus (Ci), which is crucial for the Hh pathway, is specifically expressed in the A compartment (6). In the absence of Hh, the 12-transmembrane protein Patched (Ptc) inhibits the activity of Smoothened (Smo), a seven-transmembrane protein. Full-length Ci is retained in the cytoplasm by Sufu and Cos2, where it is phosphorylated by several kinases (7). The Slimb-Cul1 E3 ligase recognizes the phosphorylated Ci, resulting in its partial degradation to form an N-terminal truncate Ci-75 (8, 9). Due to lack of the activating domain (AD), Ci-75 enters the nucleus to repress target gene expression (10, 11). When Hh is present, it relieves the inhibitory effect of Ptc on Smo, allowing full-length Ci to translocate into the nucleus and activate the expression of Hh-responsive genes, such as *dpp*, *ptc,* and *en* (12, 13). In addition, our previous study has revealed that Hh stabilizes Ci by enhancing its binding to the deubiquitinase Usp7 (14). Therefore, Hh regulates Ci through multiple mechanisms.

The activation of Hh signaling involves the movement of full-length Ci into the cell nucleus, where it binds to the promoter regions of target genes (15). Once in the nucleus, Ci plays a critical role in activating Hh-responsive genes by using its DNA binding domain to recognize promoter regions and recruiting the coactivator CBP through its AD (16, 17). This dual function of Ci is essential for proper gene expression, and any defects will disrupt its transcriptional activity. The previous study has demonstrated that Sufu is able to diminish Ci activity by reducing its affinity to CBP (18). Fused phosphorylates Ci to facilitate its interaction with CBP, thereby activating Hh signaling (19). Moreover, the amount of nuclear Ci is precisely controlled through reversible ubiquitination modifications (14, 20). However, the mechanism that regulates the affinity of Ci to promoters of target genes remains elusive.

Tai was originally identified as a key regulator of border cell migration, with mutations causing a delay in this process (21). It is the sole steroid-receptor coactivator in insects that plays a role in various physiological processes, such as metamorphosis and intestinal homeostasis (22, 23). Tai responds to juvenile hormone (JH) signals to turn on target gene expression by forming a complex with the JH receptor Methoprene-tolerant (Met)

Author contributions: Q.L. and Z.Z. designed research; X.Y., X.W., K.M., D.G., Y.D., D.Z., W.D., and Y.Z. performed research; X.Y., X.W., Q.L., and Z.Z. analyzed data; and Z.Z. wrote the paper.

The authors declare no competing interest.

This article is a PNAS Direct Submission. N.A.R.-D.G. is a guest editor invited by the Editorial Board.

[1]To whom correspondence may be addressed. Email: zhouzz@sdau.edu.cn.

This article contains supporting information online at https://www.pnas.org/lookup/suppl/doi:10.1073/pnas.2409380121/-/DCSupplemental.

Published November 12, 2024.

and recognizing the E-box element (CACGTG) on promoters (24, 25). Besides, recent studies have revealed that Tai interacts with the Hippo pathway transcriptional coactivator Yorkie (Yki) to promote the expression of not only canonical Yki-responsive genes including *cycE* and *diap1* but also germline stem cell factors such as *nanos* and *piwi* in developing somatic epithelia, ultimately leading to severe organ overgrowth (26, 27). Structurally, Tai consists of four major domains: basic-Helix-Loop-Helix (bHLH), Per-Arnt-Sim (PAS), LxxLL, and glutamine-rich domain (Poly Q) (27). It utilizes the bHLH domain to bind the E-box consensus sequence (28). Intriguingly, chromatin immunoprecipitation and microarray analysis (ChIP-chip) have shown the enrichment of E-box elements surrounding Glioma-Associated Oncogene Family Zinc Finger 1 (GLI1)-bound regions (29). In line with this, E-box elements are also present in the promoter regions of *dpp* and *ptc*, suggesting a potential functional relationship between Ci and an E-box binding protein. However, it is still unknown whether Tai collaborates with Ci to regulate target gene expression.

Mammalian genomes encode three Tai orthologs, Steroid Receptor Coactivators 1-3 (SRC1-3, also known as NCOA1-3), which have distinct but partially overlapping functions (30). Plenty of studies have demonstrated that NCOA1 and NCOA3 mainly exert protumor effects in various types of cancer (31–34). On the other hand, NCOA2 plays dual roles in tumorigenesis. A mutagenesis study has revealed that NCOA2 acts as a tumor suppressor in liver cancer (35). However, in prostate cancer, NCOA2 promotes cancer survival and metastasis by reprogramming glutamine metabolism (36). To date, the interaction between SRC1-3 and the Hh pathway in tumorigenesis is still unclear.

In this study, we identified that Tai acts as a negative regulator of the Hh pathway in *Drosophila*. Through genetic analyses, we found that Tai disrupts the reception of the Hh signal, rather than its transmission. Tai was able to prevent the upregulation of target genes and excessive organ growth caused by Ci overexpression. Tai was found to inhibit the expression of Ci target genes independently of the E-box elements near Ci-bound regions. Epistasis experiments revealed that Tai works in parallel with Ci to suppress its transcriptional activity. The LxxLL domain of Tai was identified as essential and sufficient for inhibiting the Hh pathway. Biochemical studies showed that Tai binds to Ci-DNA-binding domain (DBD) through its LxxLL domain, thereby weakening Ci's interaction with promoters of target genes. Hh treatment weakened the interaction between Ci and Tai, releasing Tai's inhibition on Ci. Intriguingly, only NCOA2, but not NCOA1 or NCOA3, was found to play a conserved role in suppressing the Hh pathway and Ci-induced overgrowth. Additionally, we demonstrated that NCOA2 interacts with GLI to inhibit the Hh pathway in mammalian cells. Overall, our study not only uncovered an additional mechanism for regulating the Hh pathway but also highlighted the distinct functions of NCOA1-3.

Results

Tai Is a Negative Regulator of the Hh Signaling Pathway. In *Drosophila* wings, the Hh pathway is involved in regulating vein development, and its hyperactivation leads to the formation of extra veins (5). To identify additional regulators of the Hh signaling pathway, we conducted a modifier screening by ectopically expressing Smo in wings using the *nub*-Gal4 driver. Consistent with the previous study (37), overexpression of Smo alone did not produce any additional veins (compare Fig. 1*B* with Fig. 1*A*), indicating that Smo is not enough to activate the Hh pathway on its own. Through an RNAi-mediated screen, we found that knockdown of *tai* (BSC36095) under *nub*>Smo background resulted in the induction of extra veins in the A compartment (Fig. 1*C*), where Ci is expressed. To rule out potential off-target effects, we used two other RNAi lines (THU4889 and THU1075) targeting different regions of the *tai* gene sequence, both of which produced a similar phenotype (*SI Appendix*, Fig. S1 *A* and *B*). The RT-qPCR assay confirmed that these RNAi lines effectively suppressed the expression of

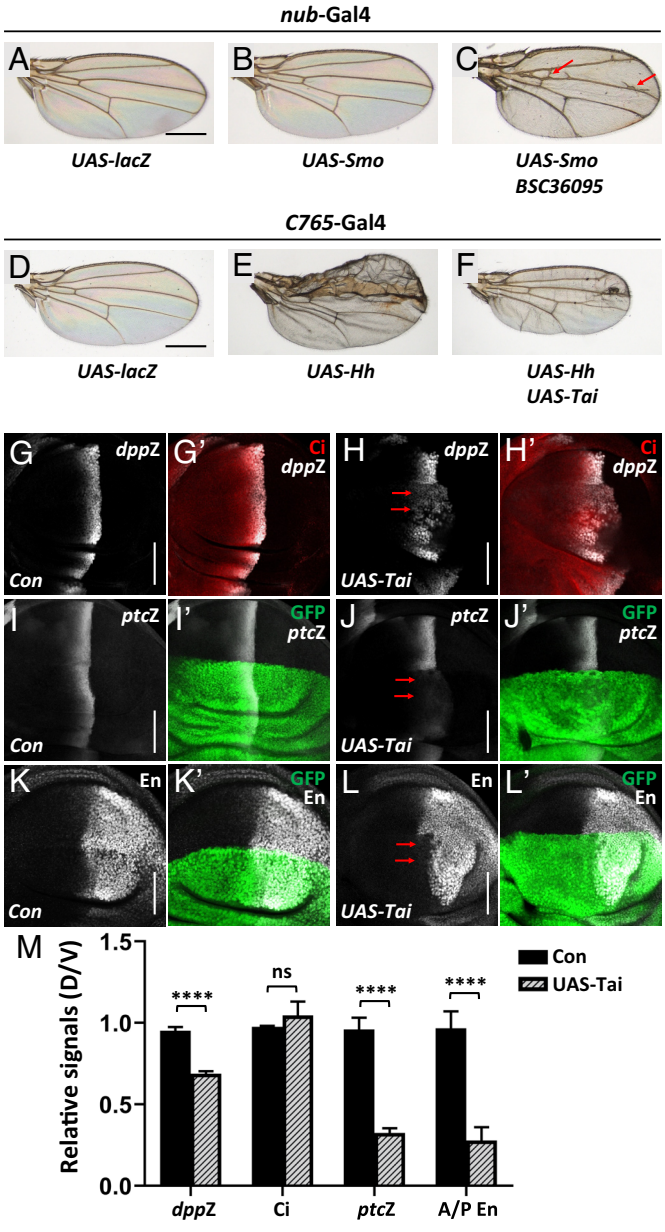

Fig. 1. Tai is a negative regulator of the Hh pathway. (*A*–*C*) Comparison of adult wings from the control (*A*), Smo overexpression by *nub*-Gal4 (*B*), and Smo overexpression plus *tai* knockdown (*C*). Overexpression of Smo did not produce detectable phenotypes, while simultaneous knockdown of *tai* led to extra veins in the A compartment (arrows). (*D*–*F*) Comparison of adult wings from the control (*D*), Hh overexpression by *C765*-Gal4 (*E*), and simultaneous overexpression of Hh plus Tai by *C765*-Gal4 (*F*). Of note, the extra veins induced by Hh overexpression in the A compartment were effectively rescued by coexpressing Tai. (*G*–*H'*) Wing discs of the control (*G* and *G'*) and Tai overexpression by *ap*-Gal4 (*H* and *H'*) were stained to show Ci (red) and *dpp*-lacZ (white). Tai overexpression led to a reduction in *dpp*-lacZ (indicated by arrows) but did not decrease Ci. (*I*–*J'*) Overexpression of Tai down-regulated the expression of *ptc*-lacZ (arrows). The GFP marks the expression pattern of *ap*-Gal4 in the wing disc. (*K*–*L'*) Tai overexpression decreased En in the A compartment adjacent to the A/P boundary (arrows). (*M*) Quantitative analyses of *G*–*L'* signals ($n = 5$). (Scale bars: 400 μm for adult wings and 50 μm for wing discs.)

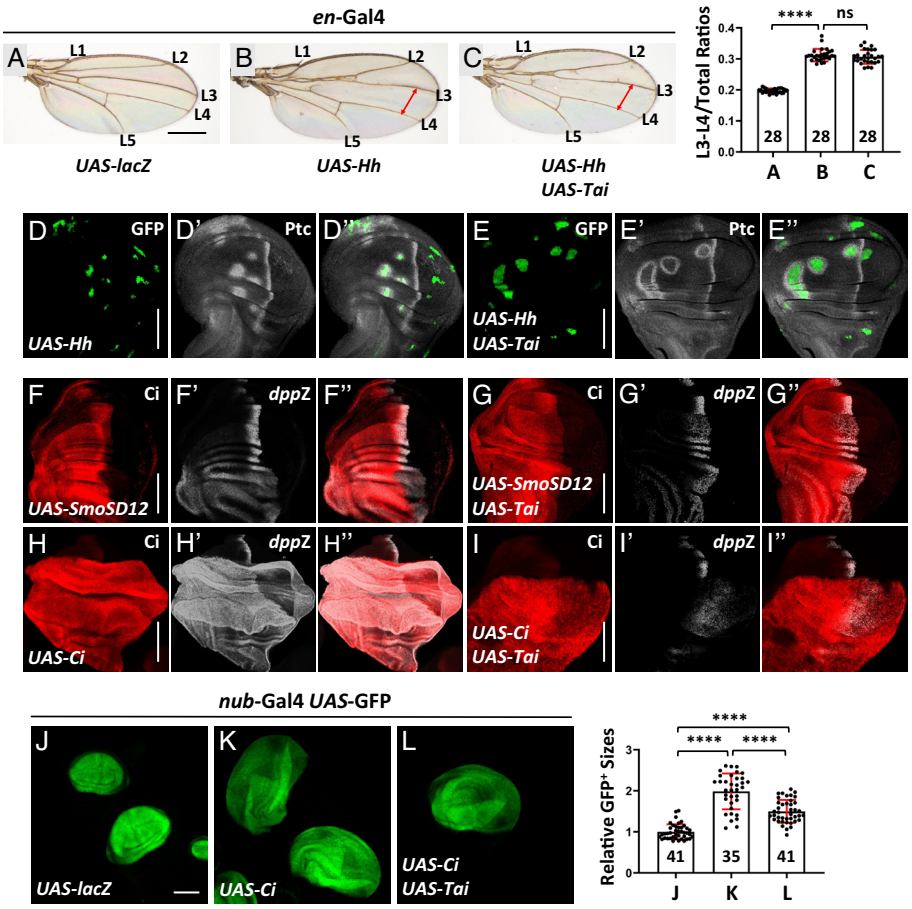

Fig. 2. Tai sits in parallel to Ci to suppress the Hh pathway. (*A–C*) Comparison of adult wings of the control (*A*), Hh overexpression by *en*-Gal4 (*B*), and coexpression of Hh and Tai (*C*). The ratios of L3/L4 areas to total wing areas were statistically analyzed on the *Right*, with the numbers in the bars indicating the number of wings that were counted. Of note, overexpression of Hh in the P compartment enlarged the L3/L4 space (*B*), which could not be restored by coexpressing Tai (*C*). (*D–E″*) Wing discs expressing Hh by *Ay*-Gal4 (*D–D″*) and coexpressing Hh plus Tai (*E–E″*) were stained to show the expression of GFP (green) and Ptc (white). GFP marks the expression pattern of *Ay*-Gal4. Ptc is activated in anterior cells in both *hh*-expressing cells (green) and the surrounding wild-type cells. Tai specifically suppresses Ptc in clone cells, suggesting that it disrupts the transduction of Hh signal. (*F–G″*) Wing discs expressing SmoSD12 by *ap*-Gal4 (*F–F″*) and coexpressing SmoSD12 plus Tai were stained with Ci (red) and *dpp*-lacZ (white). The upregulation of *dpp*-lacZ induced by SmoSD12 was counteracted by coexpressing Tai. (*H–I″*) The elevation of *dpp*-lacZ by Ci overexpression (*H–H″*) was effectively blocked by coexpressing Tai (*I–I″*). (*J–L*) Comparison of wing discs from the control (*J*), Ci overexpression (*K*), and Ci plus Tai coexpression (*L*). The expression pattern of *nub*-Gal4 in the wing discs was indicated by GFP. Quantitative analyses of the GFP areas were shown on the *Right*, with the numbers in the bars indicating the number of wing discs that were counted. Remarkably, overgrowth of wing discs induced by Ci overexpression was neutralized by coexpressing Tai. (Scale bars: 400 μm for adult wings and 100 μm for wing discs.)

endogenous *tai* (*SI Appendix*, Fig. S1*C*). Additionally, knocking down *tai* in a wild-type background using a stronger Gal4 driver resulted in extra veins and an enlarged L3/L4 space (*SI Appendix*, Fig. S1 *D* and *E*), which is a manifestation of the activation of the Hh pathway. On the other hand, overexpression of Hh in the wing using *C765*-Gal4 induced severe extra veins in the A compartment (compare Fig. 1*E* with Fig. 1*D*), which was restored by Tai coexpression (Fig. 1*F*), suggesting that Tai has the ability to suppress the Hh pathway.

After demonstrating that Tai inhibits the formation of extra veins under Hh-activated background, we investigated whether Tai also affects the expression of Hh-responsive genes. In comparison to control discs (*SI Appendix*, Fig. S1 *F*, *F'*, *H*, *H'*, *J*, and *J'*), knockdown of *tai* by expressing *tai* RNAi (BSC36095) with a dorsal compartment-specific Gal4 driver *ap*-Gal4 up-regulated the expression of Hh target genes, including *dpp*-lacZ (*SI Appendix*, Fig. S1 *G* and *G'*), *kn*-lacZ (*SI Appendix*, Fig. S1 *I* and *I'*), and Ptc (*SI Appendix*, Fig. S1 *K* and *K'*). Conversely, overexpression of Tai apparently down-regulated the expression of *dpp*-lacZ (compare Fig. 1 *H* and *H'* with Fig. 1 *G* and *G'*), *ptc*-lacZ (compare Fig. 1 *J* and *J'* with Fig. 1 *I* and *I'*), and En (compare Fig. 1 *L* and *L'* with Fig. 1 *K* and *K'*), without decreasing Ci protein levels (compare Fig. 1*H'* with Fig. 1*G'*). Remarkably, Tai specifically suppressed *en* expression near the A/P boundary, which is induced by the Hh pathway (38), while having no effect on Hh-independent *en* expression in the P compartment cells (Fig. 1*L*). This suggests that Tai reduces *en* expression by inhibiting the Hh pathway. Taken together, these findings demonstrate that Tai serves as a bona fide suppressor of the Hh pathway.

Tai Sits in Parallel with Ci to Inhibit the Hh Pathway. In order to understand the mechanism of Tai suppressing the Hh pathway, we initially examined its expression pattern. A previous study has revealed that *tai* is ubiquitously expressed during embryogenesis (39). Similarly, our fluorescence in situ hybridization (FISH) assays showed that *tai* is transcribed evenly throughout both the wing and eye discs (*SI Appendix*, Fig. S2 *A–D″*). In the wing disc, Hh protein is secreted from the P compartment to the A compartment, forming a short-range gradient (40). This gradient allows only A compartment cells near the A/P boundary to receive the Hh signal and activate target genes (5). Given that the above results have demonstrated that Tai is a suppressor of the Hh pathway, we sought to test whether Tai inhibits Hh release or Hh response. When Hh was ectopically expressed in the P compartment via *en*-Gal4, it led to an increased concentration of Hh and a wider diffusive gradient, resulting in the expansion of the L3-L4 intervein (compare Fig. 2*B* with Fig. 2*A*). However, coexpression of Tai in the P compartment did not rescue Hh-induced enhancement of L3-L4 space (compare Fig. 2*C* with Fig. 2*B*). Additionally, when Hh was overexpressed using the Flp-out technique and marked with GFP staining (41), it induced the expression of Ptc in the A compartment cells, but not in the P compartment cells (Fig. 2 *D–D″*), since P compartment cells lacked Ci. Of note, surrounding cells also showed induced Ptc expression due to Hh diffusion (Fig. 2*D'*) (42). Tai only blocked Ptc expression in cells overexpressing Hh, not in surrounding cells (Fig. 2 *E–E″*), indicating that Tai interferes with Hh response rather than Hh secretion.

To further investigate how Tai inhibits the Hh response, we performed epistatic analyses. We observed that ectopic expression of an

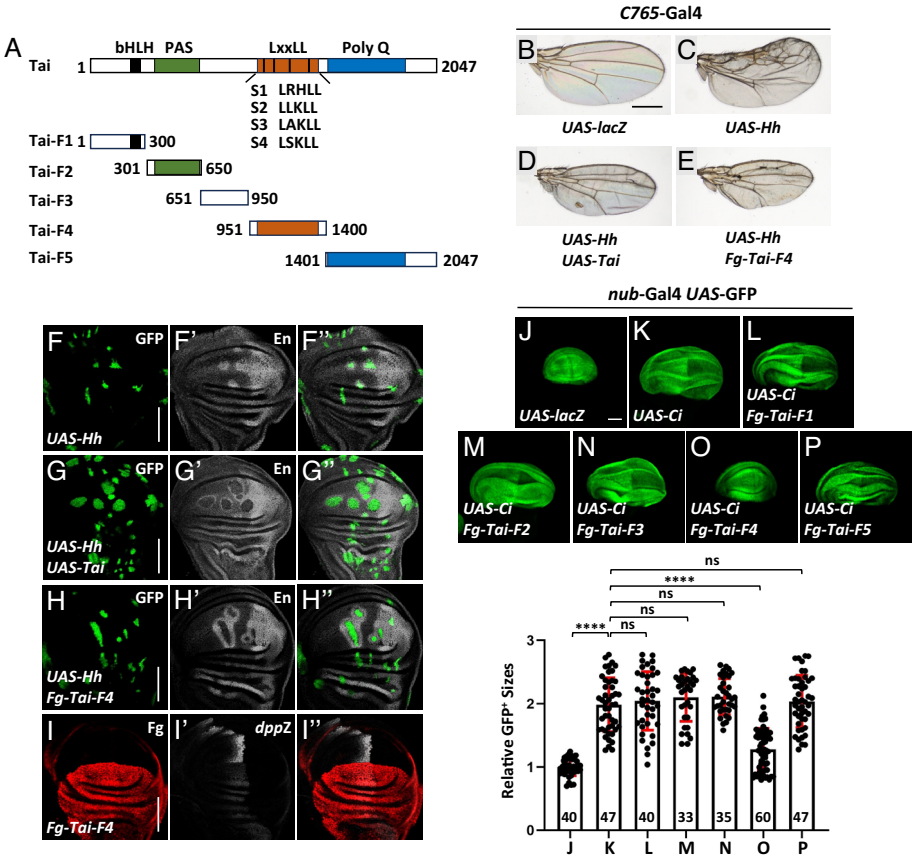

Fig. 3. Tai inhibits the Hh pathway through its LxxLL domain. (*A*) Schematic drawings show the domains and four LxxLL motifs in Tai. (*B–E*) Adult wing phenotypes from the control (*B*), Hh overexpression by *C765*-Gal4 (*C*), Hh plus Tai coexpression by *C765*-Gal4 (*D*), and Hh plus Tai-F4 coexpression (*E*). The extra wing veins induced by Hh overexpression were successfully rescued by coexpressing Tai or Tai-F4. (*F–H"*) Wing disc of Hh overexpression (*F–F"*), Hh and Tai coexpression (*G–G"*), and Hh and Tai-F4 coexpression (*H–H"*) by *Ay*-Gal4 were stained to show GFP (green) and En (white). GFP marks the expression pattern of *Ay*-Gal4. (*I–I"*) A wing disc expressing Tai-F4 by *ap*-Gal4 was immunostained with Fg (red) and lacZ (white). When Tai-F4 was overexpressed, the *dpp*-lacZ level was down-regulated. (*J–P*) Comparison of wing discs from the control (*J*), Ci overexpression (*K*), Ci plus Fg-Tai-F1 overexpression (*L*), Ci plus Fg-Tai-F2 overexpression (*M*), Ci plus Fg-Tai-F3 overexpression (*N*), Ci plus Fg-Tai-F4 overexpression (*O*), and Ci plus Fg-Tai-F5 overexpression (*P*). Quantitative analyses of the GFP areas were shown on the *Below*, with the numbers in the bars indicating the number of wing discs that were counted. Of note, the excessive growth of wing discs induced by Ci overexpression was blocked by coexpressing Tai-F4, not the other Tai mutants. (Scale bars: 400 μm for adult wings and 100 μm for wing discs.)

activated form of Smo (SmoSD12) (43) led to an increase in *dpp*-lacZ levels (Fig. 2 *F–F"*). However, coexpression of Tai prevented this upregulation (Fig. 2 *G–G"*), inferring that Tai acts downstream of Smo. Furthermore, overexpression of Ci resulted in a significant elevation in *dpp*-lacZ expression (Fig. 2 *H–H"*), which was abolished by coexpressing Tai (Fig. 2 *I–I"*). Likewise, overexpression of Ci induced ectopic expression of *ptc*-lacZ (compare *SI Appendix*, Fig. S2 *F–F"* with *SI Appendix*, Fig. S2 *E–E"*), which was also counteracted by Tai (*SI Appendix*, Fig. S2 *G–G"*), suggesting that Tai is able to suppress the transcriptional activity of Ci. Consistent with the known proliferative role of the Hh pathway (6), overexpression of Ci in wing discs resulted in excessive growth (compare Fig. 2*K* with Fig. 2*J*), which was neutralized by coexpressing Tai (Fig. 2*L*). In contrast, knockdown of *tai* exacerbated Ci-induced overgrowth of wing discs (*SI Appendix*, Fig. S2 *H–K*). Overall, Tai possibly functions in parallel with Ci to suppress its activity.

Tai Suppresses Ci Activity Independent of Met/Gce. Since Tai typically interacts with the transcription factor Met or its paralog Gce to transcribe target genes including *krh-1* (44, 45), we aimed to investigate whether Tai's inhibition of Ci depends on Met/Gce. Unlike Tai (Fig. 1 *H* and *H'*), overexpression of either Met (*SI Appendix*, Fig. S3 *A–A"*) or Gce (*SI Appendix*, Fig. S3 *B–B"*) did not decrease *dpp*-lacZ expression. In addition, neither Met nor Gce could restore the upregulation of *dpp*-lacZ induced by Ci overexpression (*SI Appendix*, Fig. S3 *C–D"*), suggesting that Met/Gce is unable to suppress Ci transcriptional activity. However, Tai was able to neutralize the enhancement of *dpp*-lacZ by Ci even in the presence of *met* knockdown (*SI Appendix*, Fig. S3 *E–E"*), indicating that Tai inhibits Ci independently of Met. Compared with the control wing disc (*SI Appendix*, Fig. S3*F*), overexpression of Ci led to overgrowth (*SI Appendix*, Fig. S3*G*), which could not be rescued by coexpressing Gce (*SI Appendix*, Fig. S3*H*) or Met (*SI Appendix*, Fig. S3*I*). In conclusion, Met and Gce are not essential for Tai to suppress Ci activity.

Tai Inhibits the Hh Pathway Through Its LxxLL Domain. To explore which domain of Tai is important for inhibiting Ci activity, we generated several transgenic flies expressing distinct domains of Tai (Fig. 3*A*). These constructs were introduced into the same genomic locus using the phiC31 integrase system to ensure consistent expression levels (41). Intriguingly, overexpression of Tai-F4, which contains the LxxLL domain, effectively rescued the formation of extra veins caused by Hh ectopic expression, phenocopying full-length Tai (Fig. 3 *B–E*). However, other truncated forms of Tai did not have the same effect (*SI Appendix*, Fig. S4 *A–D*). Both full-length Tai and Tai-F4 were able to suppress Hh-induced extra veins to a similar extent (Fig. 3 *D* and *E*), highlighting the importance of the LxxLL domain for Tai to suppress the Hh pathway. Furthermore, both full-length Tai and Tai-F4 (Fig. 3 *F–H'*), but not other truncated mutants (*SI Appendix*, Fig. S4 *E–H"*), were able to inhibit Hh-induced En expression in a cell-autonomous manner, indicating that Tai-F4 disrupts the response to the Hh signal rather than its transmission. In addition, ectopic expression of Tai-F4 down-regulated *dpp*-lacZ (Fig. 3 *I–I"*), while other truncated forms of Tai failed to do so (*SI Appendix*, Fig. S4 *I–L'*).

Having demonstrated that Tai-F4 phenocopies full-length Tai in antagonizing the Hh pathway, we sought to investigate the effect of Tai-F4 on Ci activity. The elevation of *dpp*-lacZ induced by Ci overexpression was exclusively rescued by coexpressing Tai-F4, but not by other truncates (*SI Appendix*, Fig. S4 *M–R"*). In line with this, only Tai-F4 was able to neutralize Ci-induced overgrowth (Fig. 3 *J–P*), together indicating that Tai-F4 is sufficient to suppress Ci activity. Therefore, these results demonstrate that Tai inhibits the Hh pathway through its LxxLL domain.

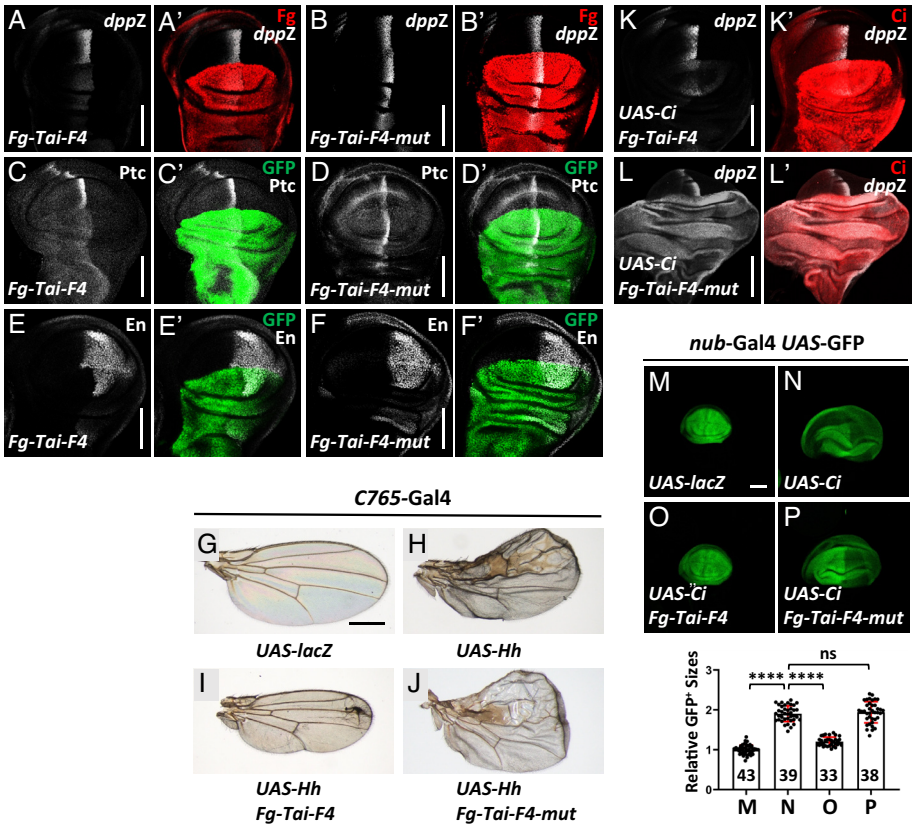

Fig. 4. LxxLL motifs are essential for Tai suppressing the Hh pathway. (*A–B'*) Wing discs expressing Fg-Tai-F4 (*A* and *A'*) or Fg-Tai-F4-mut (*B* and *B'*) were stained to show Fg (red) and *dpp*-lacZ (white). (*C–D'*) Wing discs of Fg-Tai-F4 overexpression by *ap*-Gal4 (*C* and *C'*) and Fg-Tai-F4-mut overexpression (*D* and *D'*) were stained with GFP (green) and Ptc (white). GFP indicates the expression pattern of *ap*-Gal4. (*E–F'*) Wing discs from Fg-Tai-F4 overexpression (*E* and *E'*) and Fg-Tai-F4-mut overexpression (*F* and *F'*) were stained with GFP (green) and En (white). (*G–J*) Comparison of adult wings from the control (*G*), Hh overexpression by *C765*-Gal4 (*H*), Hh and Fg-Tai-F4 coexpression (*I*), and Hh and Fg-Tai-F4-mut coexpression (*J*). The extra veins caused by Ci overexpression were rescued by Tai-F4, but not Tai-F4-mut. (*K–L'*) Wing discs from simultaneous expression of Ci plus Fg-Tai-F4 via *ap*-Gal4 (*K* and *K'*) and Ci plus Fg-Tai-F4-mut overexpression (*L* and *L'*) were stained to show Ci (red) and *dpp*-lacZ (white). The upregulation of Ci overexpression was restored by Tai-F4, but not Tai-F4-mut. (*M–P*) Wing discs from the control (*M*), Ci overexpression (*N*), Ci plus Fg-Tai-F4 overexpression (*O*), and Ci plus Fg-Tai-F4-mut overexpression (*P*). Quantitative analyses of the GFP areas were shown on the *Below*, with the numbers in the bars indicating the number of wing discs that were counted. The excessive growth of wing discs induced by Ci was blocked by coexpressing Tai-F4, but not Tai-F4-mut. (Scale bars: 400 μm for adult wings and 100 μm for wing discs.)

The LxxLL Motifs Are Essential for Tai in Suppressing the Hh Pathway. Structurally, Tai-F4 contains four LxxLL motifs: LRHLL (S1), LLKLL (S2), LAKLL (S3), and LSKLL (S4) (Fig. 3*A*). Although the LxxLL domain of Tai is sufficient to inhibit the Hh pathway, it is not clear whether these LxxLL motifs are involved in this process. To this end, we utilized the phiC31 integrase system to generate a mutant transgene Tai-F4-mut, in which all leucines in the LxxLL motifs were replaced with alanines. Despite overexpression of Tai-F4 by *ap*-Gal4 apparently diminished levels of *dpp*-lacZ (Fig. 4 *A* and *A'*), Ptc (Fig. 4 *C* and *C'*), and En (Fig. 4 *E* and *E'*), Tai-F4-mut failed to do so (Fig. 4 *B*, *B'*, *D*, *D'*, *F*, and *F'*). On the other hand, extra veins caused by Hh overexpression were effectively recovered by coexpressing Tai-F4, but not Tai-F4-mut (Fig. 4 *G–J*). Moreover, compared with Tai-F4 (Fig. 4 *K* and *K'*), Tai-F4-mut did not suppress Ci-induced *dpp*-lacZ upregulation (Fig. 4 *L* and *L'*). Consistently, Ci-caused overgrowth was antagonized by Tai-F4, but not Tai-F4-mut (Fig. 4 *M–P*). Altogether, these findings suggest that the LxxLL motifs are indispensable for Tai to inhibit the Hh pathway.

Since Tai relies on its LxxLL motifs to inhibit the Hh pathway, we decided to investigate which LxxLL motif is crucial. We constructed four mutant transgenes (mS1-mS4) with mutations in the corresponding LxxLL motifs. Surprisingly, overexpression of these mutant transgenes led to a reduction in *dpp*-lacZ (*SI Appendix*, Fig. S5 *A–D"*), indicating that deleting a single LxxLL motif is insufficient to abolish Tai's inhibition on the Hh pathway. Accordingly, Ci-induced overgrowth was prevented by Tai-F4 and these four mutants, to the same extent (*SI Appendix*, Fig. S5 *E–K*).

Tai Interacts with Ci. The LxxLL motifs are typically involved in protein–protein interactions (46), speculating that Tai may inhibit the Hh pathway by interacting with one of its components. Given the above epistatic results placing Tai in parallel with Ci, we focused on the interaction between Tai and Ci. As expected, the co-IP assay revealed that Fg-Tai could pull down Myc-Ci (Fig. 5*B*). To determine the specific region in Ci responsible for interacting with Tai, we generated several truncated constructs for subsequent co-IP experiments (Fig. 5*A*). The results showed that only CiM pulled down Fg-Tai (Fig. 5*C*), suggesting that Ci binds Tai through its middle region. Additionally, Tai-F4, which phenocopied full-length Tai, was able to bind CiM (Fig. 5*D*). Specifically, CiM contains a zinc finger DBD responsible for recognizing promoters of target genes, and an AD for recruiting cofactors such as CBP (Fig. 5*A*) (16, 17). To further narrow down the Tai-interacting region in CiM, we constructed two truncated plasmids to express DBD or AD domains (Fig. 5*A*). The co-IP result revealed that CiDBD, rather than CiAD interacted with Tai-F4 (Fig. 5*E*). Since mutation of all LxxLL motifs abolished the inhibition of Tai-F4 on Ci activity, we tried to examine the interaction between Tai-F4-mut and CiM. Consistently, Tai-F4-mut almost lost the ability to pull down CiM (Fig. 5*F*), manifesting that Tai-F4 binds CiM via its LxxLL motifs. Interestingly, cotransfection of HhN decreased the interaction between Ci and Tai (Fig. 5*G*), as well as weakened the binding affinity between CiM and Tai-F4 (Fig. 5*H*).

Having demonstrated that Tai binds to Ci, we sought to explore the correlation between this interaction and Tai's function. The E3 ligase Rdx interacts with both the N terminus and C terminus of Ci to target it for degradation through ubiquitination (20). This allows CiM to evade Rdx-induced degradation, resulting in a more pronounced phenotype. Overexpression of CiM in adult eyes using *GMR*-Gal4 resulted in defects (Fig. 5*I*), which were largely recovered by coexpressing Tai (Fig. 5*J*). Both full-length Tai and Tai-F4 were able to rescue the eye defects caused by CiM, while other Tai truncates failed to do so (Fig. 5 *K–O*). However, Tai-F4-mut, lacking all LxxLL motifs, did not alleviate the eye defects (Fig. 5*P*). Taken together, these findings suggest that Tai

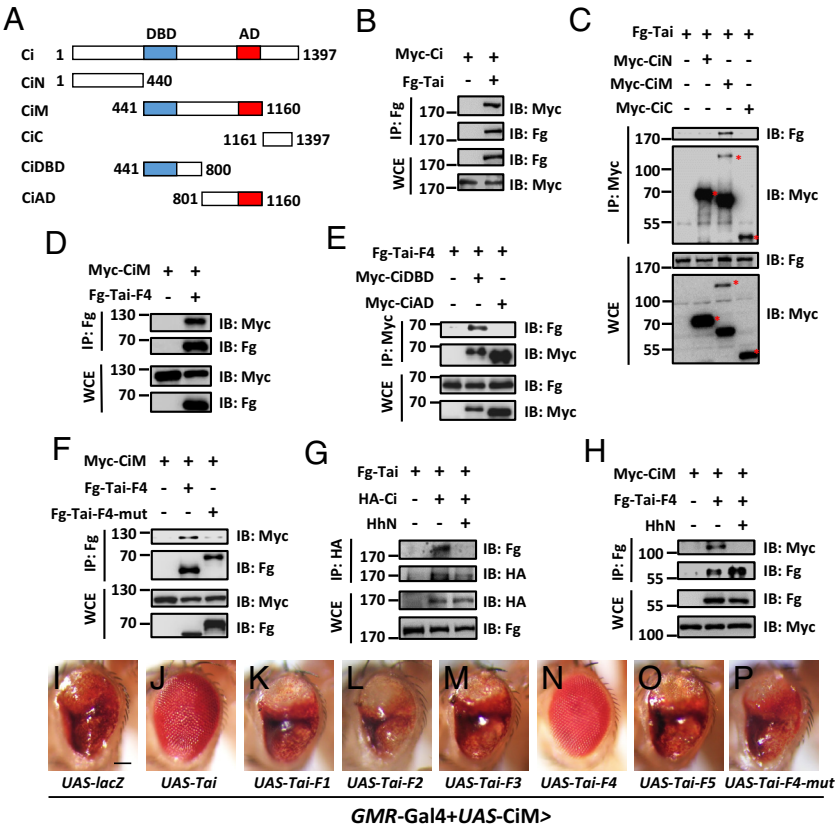

Fig. 5. Tai interacts with Ci. (*A*) Schematic drawings show the domains in Ci and its truncated fragments used in the subsequent co-IP experiments. (*B*) Immunoblots of immunoprecipitates (*Top* two panels) or whole cell extracts (WCE, *Bottom* two panels) from 293 T cells expressing indicated constructs. Of note, Fg-Tai pulled down Myc-Ci. (*C*) Myc-CiM, not Myc-CiN or Myc-CiC, interacted with Fg-Tai. (*D*) Fg-Tai-F4 pulled down Myc-CiM. (*E*) Myc-CiDBD, rather than Myc-CiAD, was able to pull down Fg-Tai-F4. (*F*) Mutation of the LxxLL motifs in Tai-F4 abolished its interaction with Myc-CiM. (*G*) Cotransfection of HhN suppressed Fg-Tai binding to HA-Ci in S2 cells. (*H*) HhN inhibited the interaction between Fg-Tai-F4 and Myc-CiM in S2 cells. (*I*–*P*) Comparison of adult eyes from indicated genotypes. Remarkably, CiM-induced eye defects (*I*) were effectively rescued by coexpressing Tai (*J*) or Tai-F4 (*N*), but not other Tai truncates (*K*, *L*, *M*, and *O*) and Tai-F4-mut (*P*). (Scale bars: 100 μm for adult eyes.)

may suppress Ci activity by binding to the DBD of Ci via its LxxLL motifs.

Tai Inhibits Ci Target Gene Expression Independently of the E-Box. A previous study has shown that E-box elements are enriched within high-confidence Gli1-bound regions (29), inferring that Gli likely works with a bHLH-containing transcription factor to activate target genes. Upon examining the promoter regions of *ptc* and *dpp*, two well-known Ci target genes, we found an E-box adjacent to the Ci binding site in each promoter (*SI Appendix*, Fig. S6*A*). To investigate the role of the E-box in Tai-mediated inhibition on Ci target genes, the luciferase reporter assay was carried out. We first constructed four luciferase reporters, with either wild-type or E-box deficient promoters inserted upstream of the luciferase sequence (*SI Appendix*, Fig. S6*A*). Dual luciferase reporter assays revealed that CiM enhanced the activities of *ptc*-Luc and *dpp*-Luc, which were counteracted by Tai (*SI Appendix*, Fig. S6*B*). However, Tai was also able to neutralize CiM-induced activation of *ptc*-m-Luc and *dpp*-m-Luc (*SI Appendix*, Fig. S6*B*), suggesting that Tai inhibits *ptc* and *dpp* regardless of their E-box elements. To validate this result in vivo, *ptc*-WT-lacZ and *ptc*-Mu-lacZ reporter flies were generated, with or without the E-box in *ptc* promoter. Both lacZ reporters were introduced into the same locus using the phiC31 integrase system to ensure equal basal expression levels (41). As expected, *ptc*-WT-lacZ expression was restricted to A/P boundary cells (*SI Appendix*, Fig. S6 *C* and *C'*), resembling the endogenous *ptc* expression pattern. Overexpression of the active form of Ci (Ci^{3P}), with three PKA kinase site mutations (47), robustly induced *ptc*-WT-lacZ misexpression (*SI Appendix*, Fig. S6 *D* and *D'*). Coexpression of Tai effectively counteracted the upregulation of *ptc*-WT-lacZ by Ci^{3P} (*SI Appendix*, Fig. S6 *E* and *E'*). On the other hand, Ci^{3P} up-regulated *ptc*-Mu-lacZ expression (compare *SI Appendix*, Fig. S6 *G* and *G'* with *SI Appendix*, Fig. S6 *F* and *F'*), which was completely abolished by Tai (*SI Appendix*, Fig. S6 *H* and *H'*). Therefore, these data demonstrate that Tai suppresses Ci target gene expression independently of the presence of E-box elements.

Tai Attenuates Ci Binding to Promoters of Target Genes. The results presented above show that Tai binds to Ci-DBD through its LxxLL domain, prompting us to examine whether Tai disrupts Ci's binding to DNA. To this end, we created a UAS-Ci-DBD-Gal4-AD transgenic fly by fusing the Gal4-AD to the C terminus of Ci-DBD (aa428-633). Overexpression of Ci-DBD-Gal4-AD resulted in an increase in Ptc protein (Fig. 6 *A*–*A"*), which was almost completely inhibited by coexpressing full-length Tai (Fig. 6 *B*–*B"*) or Tai-F4 (Fig. 6 *C*–*C"*), demonstrating that Tai suppresses Ci's activity by targeting its DBD. Additionally, both Tai-F4 and Myc-Ci-DBD-Gal4-AD were predominantly localized in the nucleus (*SI Appendix*, Fig. S6 *I*–*J"*), indicating that the inhibition of Ci-DBD-Gal4-AD by Tai-F4 takes place within the nucleus. Considering that Ci utilizes its DBD to recognize DNA for transcription, the inhibitory effect of Tai on Ci-DBD may extend to other Ci target genes. To test this possibility, we performed RNA-seq analysis to assess the broad impact of Tai on Ci's transcriptional profile. Wing discs from control flies (*MS1096*-Gal4), flies overexpressing Ci (*MS1096*>Ci), and flies coexpressing Ci and Tai (*MS1096*>Ci+Tai) were collected for RNA-seq. Compared with the control group, overexpression of Ci altered the gene expression profile, which was largely rescued by coexpressing Tai (Fig. 6*D*). Specifically, Ci overexpression up-regulated 262 genes by more than 1.5 times, whereas simultaneous overexpression of Ci and Tai only activated 138 genes (Fig. 6*E*). By comparing these two sets of up-regulated genes, most known Ci transcription targets (such as *dpp*, *ptc*, *kn*, *rdx*, *ato*, and *vn*) were exclusively clustered in

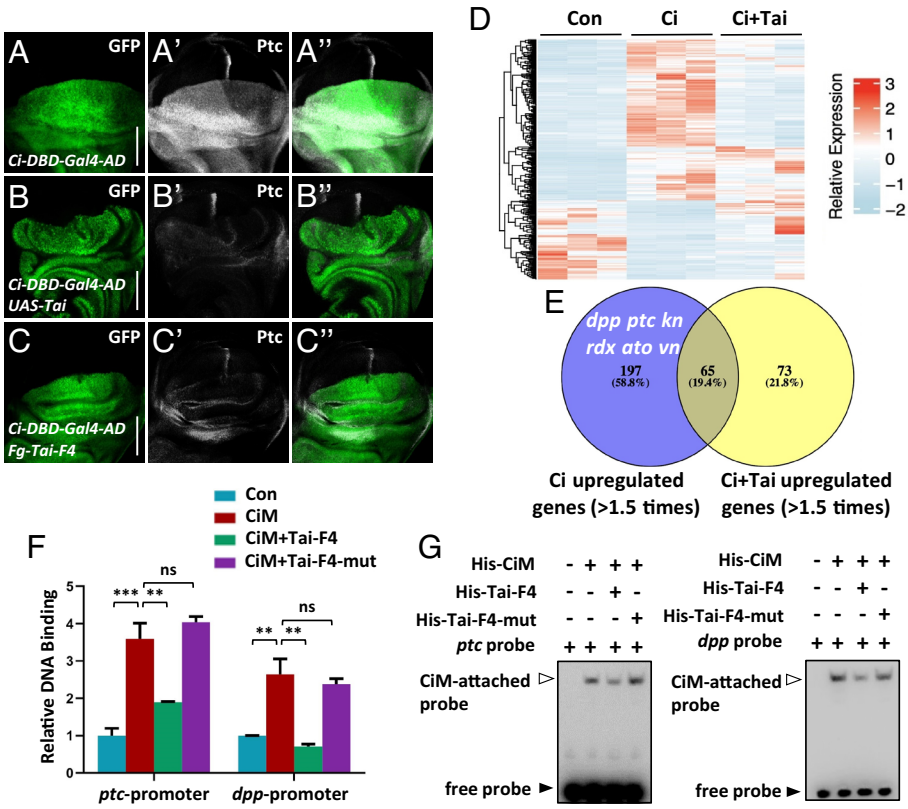

Fig. 6. Tai attenuates Ci binding to promoters of target genes. (*A–A″*) A wing disc expressing Ci-DBD-Gal4-AD by *ap*-Gal4 was stained with GFP (green) and Ptc (white). Ci-DBD-Gal4-AD could trigger ectopic expression of Ptc. (*B–C″*) Wing discs simultaneously expressing Ci-DBD-Gal4-AD and Tai (*B–B″*) or Fg-Tai-F4 (*C–C″*) were stained to show GFP (green) and Ptc (white). Of note, the enhancement of Ptc by Ci-DBD-Gal4-AD was restored by Tai or Tai-F4. (*D*) Heat map analysis of the differentially expressed genes in control (*MS1096*-Gal4), Ci overexpression (*MS1096*-Gal4>UAS-Ci), and Ci plus Tai overexpression (*MS1096*-Gal4>UAS-Ci+UAS-Tai) wing discs. (*E*) A Venn diagram showing the comparison between Ci-activated genes and Ci+Tai-activated genes. The well-known Ci transcriptional target genes were exclusive to the Ci overexpression group. (*F*) ChIP-qPCR analysis showed the enrichment of Myc-CiM on the promoters of *ptc* and *dpp* in S2 cells. Tai-F4, but not Tai-F4-mut reduced the binding of CiM to the promoters of *ptc* and *dpp*. The data are presented as means ± SD from three independent experiments. (*G*) EMSA results revealed that His-Tai-F4, rather than His-Tai-F4-mut, weakened the binding of CiM to the promoters of *ptc* and *dpp*. (Scale bars: 100 μm for wing discs.)

the Ci-overexpressed group, not in the Ci+Tai-overexpressed group (Fig. 6*E*), suggesting that Tai likely suppresses the basic transcriptional activity of Ci.

The broad impact of Tai on inhibiting the expression of Ci target genes led us to investigate whether Tai reduces the binding affinity of Ci to DNA. Initially, we employed ChIP-qPCR to evaluate the interaction between Ci and DNA. It was observed that CiM successfully pulled down the promoters of *ptc* and *dpp*, which was effectively hindered by Tai-F4, rather than Tai-F4-mut (Fig. 6*F*). These findings were further confirmed in wing discs (*SI Appendix*, Fig. S6*K*). Additionally, electrophoretic mobility-shift assays (EMSAs) validated that the direct interactions between CiM and *ptc* or *dpp* promoters were weakened by Tai-F4, not Tai-F4-mut (Fig. 6*G*). To distinguish whether Tai-F4 prevents CiM from binding to DNA or dissociates CiM from the CiM–DNA complex, we manipulated the order of incubation of Tai-F4 with the CiM and DNA probes. When Tai-F4, DNA probes, and CiM were incubated simultaneously, Tai-F4 reduced the affinity between CiM and DNA (*SI Appendix*, Fig. S6*L*). However, when CiM and DNA probes were incubated prior to adding Tai-F4, it did not decrease CiM–DNA interactions (*SI Appendix*, Fig. S6*L*), suggesting that Tai-F4 cannot dissociate the existing CiM–DNA complex. In conclusion, Tai binds to Ci to interfere with its interaction with DNA, consequently suppressing the global expression of Ci target genes.

NCOA2 Plays a Conserved Role in Inhibiting the Hh Pathway. Since key components and regulatory mechanisms of the Hh pathway are highly conserved from *Drosophila* to mammals (48), we sought to investigate whether the impact of Tai on Ci was also conserved in mammalian systems. To do this, we generated three transgenic flies, each carrying human NCOA1, NCOA2, and NCOA3. Overexpression of NCOA1 (*SI Appendix*, Fig. S7 *A–A'*) or NCOA3 (*SI Appendix*, Fig. S7 *B–B"*) did not influence *dpp*-lacZ expression, while overexpression of NCOA2 resulted in a decrease in *dpp*-lacZ level (Fig. 7 *A–A"*), similar to the effect of Tai overexpression (Fig. 1 *H* and *H'*). Furthermore, coexpression of NCOA2 was able to restore Ci-induced upregulation of *dpp*-lacZ (compare Fig. 7 *C–C"* with Fig. 7 *B–B"*), whereas NCOA1 and NCOA3 did not have the same effect (*SI Appendix*, Fig. S7 *C–D"*). NCOA2 was the only one capable of blocking Ci-induced overgrowth of wing discs (*SI Appendix*, Fig. S7 *E–I*). On the other hand, overexpression of CiM by *GMR*-Gal4 led to defective eyes (Fig. 7*D*), which was effectively recovered by NCOA2 (Fig. 7*F*), rather than NCOA1 (Fig. 7*E*) or NCOA3 (Fig. 7*G*). Thus, these findings suggest that NCOA2 plays an analogous role to Tai in inhibiting Ci's transcriptional activity.

Although the data above clearly reveal that NCOA2 inhibits Ci, it is still uncertain whether NCOA2 also suppresses GLI2, the mammalian ortholog of Ci. Overexpression of human GLI2 in the wing disc by *MS1096*-Gal4 led to ectopic activation of *ptc*-lacZ (Fig. 7 *H–H'*), similar to Ci overexpression (*SI Appendix*, Fig. S2 *F–F"*). This activation was largely reduced by NCOA2 (Fig. 7 *I–I'*), but not by NCOA1 or NCOA3 (*SI Appendix*, Fig. S7 *J–K"*), suggesting that only NCOA2 has the ability to inhibit GLI2 activity. This is further supported by the co-IP assay, which showed that NCOA2 was able to pull down GLI2, while NCOA1 and NCOA3 could not (*SI Appendix*, Fig. S7*L*).

We next determined whether NCOA2 is involved in the inhibition of GLI activity in mammalian cells. First, we examined whether NCOA2 interacts with different GLI proteins by expressing Fg-tagged NCOA2 and Myc-tagged GLI constructs in 293 T cells and carried out co-IP experiments. The results revealed that NCOA2 could bind GLI1, GLI2, and GLI3 (Fig. 7*J*). In addition, endogenous NCOA2 was able to pull down endogenous GLI proteins in 3T3 cells (Fig. 7*K*). Treatment with recombinant human Sonic Hh protein (C24II) reduced the interactions between NCOA2 and GLI proteins (Fig. 7*L*), while the Hh pathway inhibitor (cyclopamine)

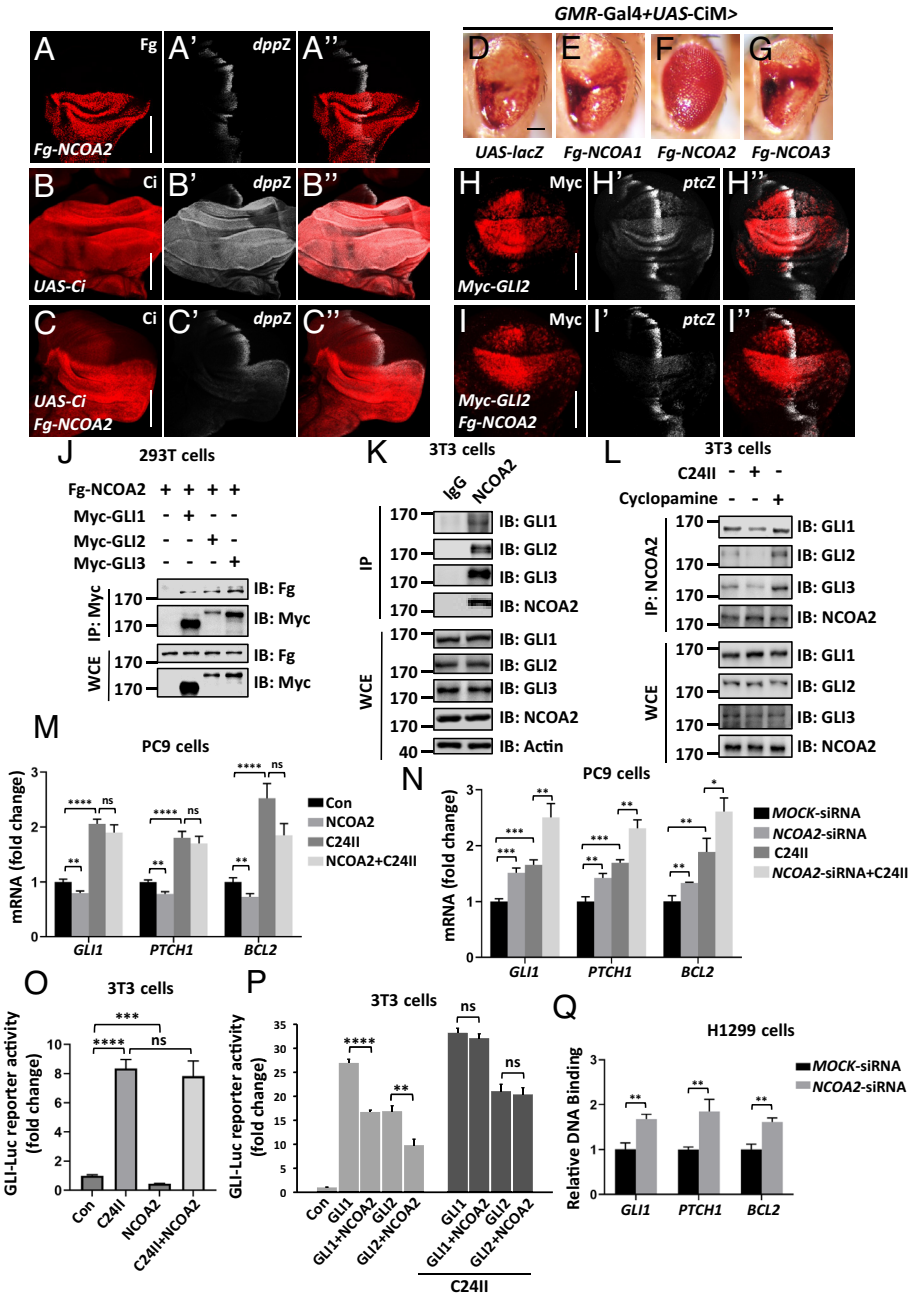

Fig. 7. NCOA2 plays a conserved role in inhibiting the Hh pathway. (*A–A″*) A wing disc expressing Fg-NCOA2 was stained to show Fg (red) and *dpp*-lacZ (white). Overexpression of NCOA2 led to a reduction in *dpp*-lacZ. (*B–C″*) Wing discs from Ci overexpression (*B–B″*) and Ci plus NCOA2 overexpression (*C–C″*) were stained with Ci (red) and *dpp*-lacZ (white). The upregulation of *dpp*-lacZ by Ci was effectively restored by coexpressing NCOA2. (*D–G*) Comparison of adult eyes of the control (*D*), Fg-NCOA1 overexpression (*E*), Fg-NCOA2 overexpression (*F*), and Fg-NCOA3 overexpression (*G*). Notably, only NCOA2 rescued CiM-induced eye phenotypes. (*H–I″*) Wing discs expressing GLI2 alone (*H–H″*), GLI2 plus NCOA2 (*I–I″*) by *MS1096*-Gal4 were stained with Myc (red) and *ptc*-lacZ (white). The activation of *ptc*-lacZ by GLI2 was neutralized by coexpressing NCOA2. (*J*) Fg-NCOA2 was able to pull down Myc-GLI1, Myc-GLI2, and Myc-GLI3 in 293T cells. (*K*) Endogenous NCOA2 interacted with GLI1, GLI2, and GLI3 in 3T3 cells. (*L*) C24II reduced, while cyclopamine enhanced the interactions between NCOA2 and GLI proteins in 3T3 cells. (*M*) RT-qPCR analyses of Hh target genes. NCOA2 decreased the expression of Hh target genes, which was reversed by C24II treatment. (*N*) Knocking down NCOA2 activated Hh target genes, which was strengthened by C24II treatment. (*O*) Dual luciferase reporter assays showed that NCOA2 inhibited GLI-Luc activity. C24II was able to abolish this inhibition. (*P*) The enhancement of GLI-Luc by GLI1 or GLI2 was diminished by coexpressing NCOA2. C24II treatment could eliminate this inhibitory effect. (*Q*) Analysis using ChIP-qPCR revealed that depletion of *NCOA2* resulted in an increase in GLI2 binding to the promoters of target genes. (Scale bars: 100 μm for adult eyes and 100 μm for wing discs.)

promoted these interactions (Fig. 7*L*). These findings were validated using exogenously expressed Fg-NCOA2 and Myc-GLI proteins (*SI Appendix*, Fig. S8 *A–F*), suggesting that the Hh pathway suppresses the interactions between NCOA2 and GLI proteins.

Considering the tumorigenicity of the Hh pathway, we selected non–small cell lung cancer (NSCLC) cell lines for subsequent studies, as NSCLC cells are responsive to this pathway (49). The co-IP experiments showed that GLI2 was able to interact with NCOA2 in both A549 cells (*SI Appendix*, Fig. S7*M*) and H1299 cells (*SI Appendix*, Fig. S7*N*). RT-qPCR assays showed that NCOA2 decreased the expression of Hh target genes, which was rescued by C24II treatment (Fig. 7*M*). Conversely, silencing *NCOA2* activated Hh target genes regardless of Shh presence (Fig. 7*N*). The effectiveness of *NCOA2*-small interfering RNA (siRNA) was confirmed through immunoblotting (IB) (*SI Appendix*, Fig. S8 *G* and *H*). Furthermore, we performed GLI-Luciferase reporter assays in 3T3 cells with or without Shh treatment (14). NCOA2 substantially decreased GLI-Luc activity, which was counteracted by Shh (Fig. 7*O*). The upregulation of GLI-Luc activity by GLI proteins was effectively suppressed by coexpressing NCOA2, and Shh treatment could remove this inhibitory effect (Fig. 7*P*). On the other hand, knockdown of *NCOA2* promoted GLI2 binding to the promoters of target genes in both H1299 cells (Fig. 7*Q*) and PC9 cells (*SI Appendix*, Fig. S8*I*). In contrast, overexpression of NCOA2 inhibited GLI2 binding to promoters, which was restored by Shh treatment (*SI Appendix*, Fig. S8*J*). Finally, the EdU incorporation assay revealed that only NCOA2, not NCOA1 or NCOA3, restrained the proliferative property of GLI2 in both A549 cells and SPCA-1 cells (*SI Appendix*, Fig. S8 *K* and *L*). Taken together, these findings strongly suggest that NCOA2 plays a conserved role in antagonizing the Hh pathway by preventing GLI interaction with DNA in mammalian cells.

Discussion

The Hh pathway is essential for the development and maintenance of various tissues and organs, and its dysfunction has been linked to a range of human diseases, including cancer (3). It is not difficult to understand that cells have evolved multiple mechanisms to keep the homeostasis of the Hh pathway, preventing its abnormal activation. During Hh signaling transduction, all upstream signals ultimately converge on the transcription factor Ci (7), making it crucial to control Ci activity for proper signal output. Here, we uncovered a mechanism to limit Ci activity, in which Tai associates with the DBD of Ci to restrain its occupancy on the promoter regions of target genes. The LxxLL motifs of Tai are necessary and sufficient for its inhibition on Ci's transcriptional activity. Intriguingly, the interaction between Tai and Ci is weakened by Hh treatment, thereby liberating Ci. Although the human genome encodes three homologs of Tai, only NCOA2 plays a conserved role in suppressing the Hh pathway in mammalian cells. Finally, NCOA2 is able to attenuate GLI2-induced cell proliferation in NSCLC cells. In summary, our study not only reveals an additional regulatory mechanism in which Hh activates Ci by inhibiting the Ci-Tai interaction but also highlights NCOA2 as a promising therapeutic target for Hh-related cancers.

The activation of Ci relies on its translocation from the cytoplasm to the nucleus, a process that is regulated by Hh signaling. When the Hh pathway is turned on, Ci is moved into the nucleus with the aid of Transportin (Trn), but this movement is impeded by Sufu (50, 51). However, removal of Sufu is insufficient to activate Ci target genes, such as *ptc*-lacZ (52), indicating that a mechanism exists to limit the transcriptional activity of nuclear Ci. Compared to nuclear Ci, previous studies pay more attention to the regulation of cytoplasmic Ci. In the absence of Hh signaling, Ci is tethered in the cytoplasm primarily by interacting with Cos2 and Sufu (53). Deletion analyses have identified a 125 amino acid domain (aa961-1065) of Ci, referred to as CORD (Cos2 responsive domain), that is responsible for transcriptional repression and cytoplasmic retention by Cos2 (53). Deficiency of the CORD in Ci disrupts its interaction with Cos2. On the other hand, Ci contains two regions (aa199-261 and aa1371-1397) that are involved in binding to Sufu (18). The activation of *ptc*-lacZ induced by Ci-DBD-Gal4-AD, without Sufu and Cos2 binding sites, is successfully rescued by Tai, indicating that Tai suppresses Ci independently of Cos2 and Sufu. In addition, our findings suggest that the inhibitory effect of Tai on Ci is likely to occur in the nucleus. Immunostaining experiments show that Tai-F4, which has an inhibitory effect on Ci, primarily localizes in the nucleus. According to previous studies, Ci possesses two nuclear localization signals (aa596-600 and aa611-614) that, when attached to cytoplasmic lacZ, induce robust nuclear localization of lacZ (54). Consistently, the Ci-DBD-Gal4-AD fusion protein, comprising aa428-633 of Ci, is mainly resided in the nucleus. The ability of Tai to neutralize the enhancement of *ptc*-lacZ by Ci-DBD-Gal4-AD demonstrates that this inhibitory effect takes place in the nucleus. Additionally, Tai specifically binds to the DBD of Ci to weaken its occupancy on DNA, strengthening the notion that Tai hinders nuclear Ci. Overall, this study uncovers a way to suppress the transcriptional activity of nuclear Ci.

The activity of Ci must be carefully controlled to prevent developmental defects or overgrowth. One way this is achieved is through the activation of the E3 ligase Rdx by Ci, which then facilitates Ci proteolysis in the nucleus, to ensure the appropriate abundance of nuclear Ci (20, 55). Here, we present an additional fail-safe mechanism to avoid overactivation of Ci by limiting its interaction with DNA. The RNA-seq analysis reveals that Tai largely counteracts the transcriptional profile of Ci overexpression, demonstrating a widespread inhibition of Ci activity. Therefore, cells possibly have developed dual safeguarding strategies to restrict excessive activation of nuclear Ci by promoting Ci degradation and inhibiting Ci-DNA interactions, respectively. In comparison to Ci degradation, the latter may be more efficient, as this regulation is a reversible process that is controlled by Hh signaling. Nevertheless, the detailed mechanism of how Hh signaling decreases the Ci-Tai interaction requires further investigation in the future.

Previous studies have revealed that Tai functions as a transcriptional coactivator in various biological contexts. Initially, Tai was identified as a coactivator of the Ecdysone Receptor to activate the ecdysone pathway (21). Subsequently, Tai was found to form complexes with Met or Gce to initiate JH signaling (56, 57). Recent studies have also uncovered that Tai interacts with Yki to enhance its transcriptional activity (26, 27). In contrast to these findings, our study demonstrates that Tai can also bind to Ci and exert an inhibitory effect, suggesting that Tai's role as a coactivator or corepressor depends on its binding partners. While previous studies have shown that Tai exacerbates overgrowth in wing discs in the context of Yki overexpression (26), our observations indicate that Tai is able to counteract Ci-induced overgrowth, highlighting Tai's antiproliferative role under the condition of Ci overexpression. Hence, understanding the biological functions of Tai necessitates consideration of the genetic backgrounds in which it operates.

The human genome encodes three orthologs of Tai, NCOA1-3. NCOA1 promotes tumor progression and drug resistance by interacting with transcription factors such as HOXC11 (58), PEA3 (59), and STAT1 (60). NCOA3 mainly serves as an oncoprotein by cooperating with several transcription factors, including E2F1 (61), ATF4 (62), STAT6 (63), and AP-1 (64). In contrast to the oncogenic properties of NCOA1 and NCOA3, NCOA2 has been found to play dual roles in tumorigenesis. A previous study has clearly demonstrated that NCOA2 reprograms glutamine metabolism to promote the survival, growth, and metastasis of prostate cancer (36). However, a mutagenesis screen discovers that mice with Ncoa2 knockout are predisposed to diethylnitrosamine-induced liver tumor (35). In addition, deletion of Ncoa2 in mice is sufficient to accelerate Myc-mediated liver tumorigenesis, but the mechanism is not yet understood (65). Despite NCOA3 sharing the highest sequence homology with Tai (34), it does not play a similar role in suppressing the Hh pathway. Our study provides strong evidence to support that only NCOA2 inhibits the Hh pathway. First, only NCOA2 exhibits the ability to antagonize Ci-induced upregulation of *dpp*-lacZ and overgrowth of wing discs. Second, NCOA2 shows physical interaction with GLI2, while NCOA1 and NCOA3 do not. Third, GLI2-mediated proliferation of NSCLC cells is effectively abolished by cotransfection with NCOA2, rather than NCOA1 or NCOA3. Considering the importance of GLI in liver tumorigenesis (66), it will be valuable to investigate whether NCOA2 exerts the antitumor effect by inhibiting GLI.

Materials and Methods

DNA Constructs. To generate Myc-Ci, Fg-Tai, Myc-GLI1, Myc-GLI2, Myc-GLI3, Fg-NCOA1, Fg-NCOA2, and Fg-NCOA3 constructs, the corresponding CDS were amplified by the DNA polymerase (Vazyme, P505), and inserted them into the pUAST-Myc, pcDNA3.1-Myc, pUAST-Fg, or pcDNA3.1-Fg backbone vectors, respectively. Truncated constructs including Myc-CiN, Myc-CiM, Myc-CiC, Myc-CiDBD, Myc-CiAD, Fg-Tai-F1, Fg-Tai-F2, Fg-Tai-F3, Fg-Tai-F4, Fg-Tai-F5, and

Fg-Tai-F4-mut were made by inserting the corresponding CDS into pUAST-Myc, pcDNA3.1-Myc, pUAST-Fg, or pcDNA3.1-Fg vectors.

***Drosophila* Genetics.** UAS-lacZ, UAS-GFP, *ap*-Gal4, *nub*-Gal4, *Ay*-Gal4, *C765*-Gal4, *GMR*-Gal4, *en*-Gal4, *MS1096*-Gal4, *dpp*-lacZ, *kn*-lacZ, and *ptc*-lacZ had been described in our previous studies (67, 68). Tai-RNAi (THU4889), Tai-RNAi (THU1075), Tai-RNAi [Bloomington *Drosophila* Stock Center (BDSC #36095)], UAS-Tai (BDSC #6378), UAS-GFP (BDSC #4775), UAS-lacZ (BDSC #1776), UAS-Smo (BDSC #44620), UAS-Hh (BDSC #98448), and w^{1118} (BDSC #3605) were obtained from THFC or BDSC. UAS-SmoSD12 and UAS-Ci^{-3P} were provided by Prof. Qing Zhang' lab, Nanjing University, China. UAS-Ci was gifted from Prof. Junzheng Zhang's lab, China Agricultural University, China. UAS-V5-Met, UAS-HA-Gce, and Met-RNAi were kindly provided from Prof. Sheng Li's lab, South China Normal University, China. Fg-Tai-F1, Fg-Tai-F2, Fg-Tai-F3, Fg-Tai-F4, Fg-Tai-F5, Fg-Tai-F4-mut, Fg-Tai-F4-mS1, Fg-Tai-F4-mS2, Fg-Tai-F4-mS3, Fg-Tai-F4-mS4, UAS-CiM, Fg-NCOA1, Fg-NCOA2, and Fg-NCOA3 were generated by injecting the indicated constructs into the 68A4 attP locus (BDSC #25710) using the phiC31 integration system (41). UAS-Myc-Ci-DBD-Gal4-AD and UAS-Myc-GLI2 were created by injecting the indicated constructs into w^{1118} *Drosophila* embryos according to the previous method (14). To obtain the lacZ reporter flies, we first amplified *ptc*-promoter sequences (from −1,200 to −100) and mutational sequences and then cloned them into CPLZN, an enhancer vector that contains *hsp70* basal promoter and lacZ reporter (41). Then, these plasmids were then injected into the 25C6 attP locus (BDSC #25709) to obtain the *ptc*-WT-lacZ and *ptc*-Mu-lacZ flies. Most crosses were conducted at 25 °C, except when observing adult wings with Hh overexpression by *C765*-Gal4 and *en*-Gal4, which were carried out at 18 °C.

Immunostaining and Confocal. The immunostaining of wing and eye discs was carried out as described previously (69). Briefly, third-instar larvae were dissected in Phosphate Buffered Saline (PBS) and fixed with freshly made 4% formaldehyde in PBS for 20 min at room temperature. After fixation, the larvae were washed three times with PBS supplemented with 0.1% Triton X-100 (PBT). Subsequently, the larvae were incubated overnight with primary antibodies in PBT at 4 °C, followed by three washes with PBT and a 2 h incubation with fluorophore-conjugated secondary antibodies at room temperature. After being washed with PBT for three times, the imaginal discs were separated and soaked in 40% glycerol. Images were captured using the Zeiss confocal microscope. The primary antibodies used in this study were as follows: rat anti-Ci (1:10, Developmental Studies Hybridoma Bank, DSHB); mouse anti-Ptc (1:10, DSHB); mouse anti-En (1:10, DSHB); rabbit anti-β Gal (1:500, Santa Cruz); mouse anti-Myc (1:200, Santa Cruz); and mouse anti-Fg (1:500, Sigma). All secondary antibodies (Jackson ImmunoResearch) were diluted 1:500 for use in this study.

FISH Assay. To synthesize RNA probes for FISH, digoxigenin-labeled uracil (U) (Roche) was used for in vitro transcription. The *tai* probe encompassed the 601-800 base pair region (starting from ATG) of the coding sequences (CDS). The sense probe was transcribed with a T7 promoter, while the antisense probe was transcribed using an SP6 promoter. We utilized SP6 RNA polymerase (Thermo Scientific) and T7 RNA polymerase (TransGen Biotech) to catalyze the synthesis of single-stranded RNA probes and purified them with ethanol following the manufacturer's instructions.

Wing and eye imaginal discs of 3rd instar larvae were dissected in PBS and immediately fixed in freshly made 4% formaldehyde in PBS for 20 min at room temperature, then dehydrated with ethanol. The specimens were incubated in PBT/proteinase K for 5 min with gentle rocking. After three washes with PBT, the prehybridization solution was added and incubated at 55 °C for 1 h. The prehybridization solution was removed and replaced with the hybridization buffer containing the probe, incubated at 55 °C for 16 to 20 h. The specimens were washed three times with PBT and incubated with anti-digoxin-coupled FITC monoclonal antibody (Sigma). Finally, imaginal discs were separated and mounted with 40% glycerol. Images were captured using the Zeiss confocal microscope.

Western Blotting and Immunofluorescence. *Drosophila* S2 cells were maintained in serum-free insect cell culture medium (HyClone) supplemented with 1% penicillin/streptomycin (Sangon Biotech) at 25 °C. The 293 T, 3T3, and four NSCLC cell lines (A549, H1299, PC9, and SPCA-1) were purchased from the American Type Culture Collection (Manassas, VA, USA) and cultured in DMEM or RPMI1640 medium (Gibco) supplemented with 10% Fetal Bovine Serum and 1% penicillin/streptomycin. Mammalian cells were cultured at 37 °C with 5% CO_2. Plasmids were transfected using PEI (Sigma) or Lipo2000 (Thermo Fisher Scientific) according to the manufacturer's instructions. For Hh activation or inhibition, cells were treated with 100 ng/mL C24II (MedChemExpress, HY-P7407) (70) or 20 μM cyclopamine (MedChemExpress, HY-17024) (71) for 24 h before cell harvesting. 48 h after transfection, cells were collected for immunoprecipitation (IP) or immunoblotting (IB) analyses following standard protocols (67). The antibodies used were mouse anti-Myc (1:2,000; Santa Cruz, sc-40), mouse anti-Fg (1:5,000; Sigma, F3165), mouse anti-HA (1:2,000; Santa Cruz, sc-7392), mouse anti-GLI1 (1:2,000; Proteintech, 66905-1-Ig), mouse anti-GLI2 (1:2,000; Santa Cruz, sc-271786), rabbit anti-GLI2 (1:2,000; Proteintech, 28245-1-AP), rabbit anti-GLI3 (1:2,000; ABclonal, A3300), rabbit anti-NCOA2 (1:2,000; ABclonal, A10280), goat anti-mouse HRP (1:10,000; Abmax), and goat anti-rabbit HRP (1:10,000; Abmax).

For EdU incorporation assays, transfected SPCA-1 and A549 cells were plated on chamber slides and incubated with 10 μM EdU (CellorLab) for 2 h before cell harvesting. Subsequently, the cells were fixed and washed according to the manufacturer's instructions. Following this, the cells were incubated with DAPI (1:1,000, Sigma) for 20 min at room temperature in the dark. Finally, the cells on slides were mounted with 40% glycerol, and images of cells were visualized and captured using the Zeiss confocal microscope.

Luciferase Reporter Assays. For luciferase experiments, the *ptc/dpp* wild-type or E-box deficient promoters were amplified and then inserted into the pGL3-Basic-Luc vector to generate *ptc*-Luc, *dpp*-Luc, *ptc*-m-Luc, and *dpp*-m-Luc. To assess GLI-mediated transcriptional activation, we employed the 8xGLI-BS-Luc reporter (72), which contains eight repeated GLI binding elements upstream of luciferase. 293 T cells were transfected with the indicated plasmids. 48 h after transfection, cells were lysed with passive lysis buffer following the standard procedure. The luciferase activity was measured using the Dual-Luciferase Reporter assay (Vazyme). The luciferase activity data are presented as means ± SD of values from at least three experiments.

RNA-seq Assay. Flies of *MS1096*-Gal4, *MS1096*-Gal4>UAS-Ci and *MS1096*-Gal4>UAS-Ci+UAS-Tai were raised at 25 °C. Total RNA was extracted from wing discs of third instar larvae by TRIzol reagent (Invitrogen) according to the standard protocol. RNA sequencing was conducted by BGI, and only high-quality reads were collected for further analysis. Differentially expressed genes were identified based on the adjusted $P < 0.01$ and the $\log_2$ fold change (FC) > 0.5.

Electrophoretic Mobility Shift Assays. Biotin-labeled *ptc* and *dpp* probes were synthesized through PCR-mediated DNA amplification, with biotin attached to the upstream of forward primers. CiM, Tai-F4, and Tai-F4-mut were cloned into the pET-32a vector for expression as fusion proteins in *Escherichia coli*. The fusion proteins were purified using IDA-Ni magnetic beads, and EMSA experiments were carried out using the Chemiluminescent EMSA kit (Beyotime) according to the manufacturer's instructions.

ChIP-qPCR Assays. Indicated plasmids or siRNA were transfected into S2, PC9, or H1299 cells. 48 h after transfection, the cells were harvested and treated with 4% formaldehyde for 10 min at room temperature to cross-link the chromatin. After washing with PBS, the cells were lysed in a buffer (5 mM PIPES, pH 8.0, 85 mM KCl, and 0.5% NP40) with protease inhibitor (MedChemExpress) and PMSF (Sigma). The chromatin was sheared by sonication for proper cycles at 4 °C and then incubated with mouse anti-Myc or mouse anti-GLI2 antibodies for 2 h. Subsequently, protein A/G agarose beads (Santa Cruz) were added at a 1:200 dilution and incubated for another 2 h. The beads were washed three times with cell lysis buffer and subjected to reverse cross-linking at 65 °C for 6 h. The DNA obtained from IP was quantified using qPCR. For ChIP-qPCR assay using wing discs, the third-instar larvae were dissected in PBS and fixed with freshly made 4% formaldehyde in PBS for 20 min at room temperature. After washing with PBS, the imaginal discs were separated in lysis buffer. A subsequent process was carried out as the above steps. The primers used in the ChIP-qPCR assays were as follows: *ptc*-promoter, 5′-CCC CCA AAC AAA TAC ACA C-3′ (forward) and 5′-TTG CCA CTG TAG TTT ATT T-3′ (reverse); *dpp*-promoter, 5′-CGA ACG CCT CTT GCC ATC-3′ (forward) and 5′-GGA AAA TTG TAA TTT CCT AG-3′ (reverse); *GLI1*-promoter, 5′-AAC TGG GTG GGG AGA A-3′ (forward) and 5′-CTG GGT TTA AGC GGT C-3′ (reverse); *PTCH1*-promoter, 5′-AGT GCG GGC CGG ATC T-3′ (forward) and

5′-TGG GCT CAC CCA CAG A-3′ (reverse); *HHIP1*-promoter, 5′-AGG ATC CAT GAC AGC TGG A-3′ (forward) and 5′-GGT CTC CCT GGC TGC AG-3′ (reverse); *BCL2*-promoter, 5′-ATG AGG TCA AGA GTT TGA GA-3′ (forward) and 5′-TGG GAT TAC AGG TGC C-3′ (reverse). Data are presented as means ± SD from three independent experiments.

RNA Interference. We employed siRNA to silence endogenous *NCOA2* in both H1299 and PC9 cells. The siRNAs were synthesized by GenePharma, and the sequences were as follows: *MOCK*-siRNA: 5′-UUC UCC GAA CGU GUC ACG UdTdT-3′ (14) and *NCOA2*-siRNA: 5′-GGG CUG UUA ACA UUA GCA AdTdT-3′ (73). Transfection of siRNAs (50 nM) was carried out using Lipofectamine 2000 following the manufacturer's instructions. After transfection with siRNAs for 72 h, cells were harvested, and the knockdown efficiency was assessed by IB.

RNA Extraction and RT-qPCR. Total RNA was isolated from cultured cells using TRIzol (Invitrogen) following standard protocols, and subsequently reverse transcribed with HiScript® Q RT SuperMix with gDNA wiper (Vazyme) according to the manufacturer's instructions. Real-time PCR was performed on ZY/VQ-100A (Yuanzan) using the ChamQ SYBR® Color qPCR Master Mix (Q711, Vazyme). The primers used for RT-qPCR were as follows: *GLI1*, 5′-AGC CTT CAG CAA TGC CAG TGA C-3′ (forward) and 5′-GTC AGG ACC ATG CAC TGT CTT G-3′ (reverse); *PTCH1*, 5′-ACC GGG ACT ATC TGC ACC G-3′ (forward) and 5′-GCC AGT AGC CTT CCC CTT G-3′ (reverse); *BCL2*, 5′-GAT AAC GGA GGC TGG GAT GC-3′ (forward) and 5′-TCA CTT GTG GCC CAG ATA GG-3′ (reverse); *ACTIN*, 5′-GAT CAT TGC TCC TCC TGA GC-3′ (forward) and 5′-ACT CCT GCT TGC TGA TCC AC-3′ (reverse). Relative quantification was analyzed by the comparative $2^{-\Delta\Delta Ct}$ method, and the results are presented as the mean ± SD of values from at least three experiments.

Statistical Analysis. The sizes of adult wings and GFP^+ areas of imaginal wing discs were measured using Image J software. All data shown in the figures were representative of three or more independent replicates and were displayed as means ± SD. Statistical significance was determined through a two-tailed unpaired Student's *t* test using Prism software (GraphPad), with significance values set at $*P < 0.05$, $**P < 0.01$, $***P < 0.001$, $****P < 0.0001$, and ns (not significant, $P > 0.05$).

Data, Materials, and Software Availability. All materials used in this study, including fly stocks, plasmids, cell lines, and antibodies, are available from the corresponding author upon request. All other data are included in the article and/or *SI Appendix*.

ACKNOWLEDGMENTS. We sincerely thank Dr. Dezhen Peng, the founder of Yuanzan Lifescience Co., Ltd., for donating a quantitative PCR instrument (ZY/VQ-100A) to our lab. We also appreciate Prof. Sheng Li, Prof. Qing Zhang, and Prof. Junzheng Zhang for generously providing *Drosophila* stocks. We also appreciate Shanghai Institute of Biochemistry and Cell Biology, BDSC and TsingHua Fly Center for providing flies, and DSHB at the University of Iowa for providing antibodies. This study was supported by grants from the National Natural Science Foundation of China (32270522, 32272945, and 32350710192) and the project of Double Thousand Plan in Jiangxi Province of China (09030049).

Author affiliations: [a]College of Life Sciences, Shandong Agricultural University, Tai'an 271018, China; and [b]Key Laboratory of Biodiversity Conservation and Bioresource Utilization of Jiangxi Province, College of Life Sciences, Jiangxi Normal University, Nanchang 330022, China

1. J. Jia, J. Jiang, Decoding the Hedgehog signal in animal development. *Cell Mol. Life Sci.* **63**, 1249–1265 (2006).
2. J. Briscoe, P. P. Thérond, The mechanisms of Hedgehog signalling and its roles in development and disease. *Nat. Rev. Mol. Cell Biol.* **14**, 416–429 (2013).
3. J. Jiang, C.-C. Hui, Hedgehog signaling in development and cancer. *Dev. Cell* **15**, 801–812 (2008).
4. J. J. Lee, D. P. von Kessler, S. Parks, P. A. Beachy, Secretion and localized transcription suggest a role in positional signaling for products of the segmentation gene hedgehog. *Cell* **71**, 33–50 (1992).
5. T. Tabata, T. B. Kornberg, Hedgehog is a signaling protein with a key role in patterning Drosophila imaginal. *Cell* **76**, 89–102 (1994).
6. M. Domínguez, M. Brunner, E. Hafen, K. Basler, Sending and receiving the hedgehog signal: Control by the Drosophila Gli protein Cubitus interruptus. *Science* **272**, 1621–1625 (1996).
7. J. T. Ohlmeyer, D. Kalderon, Hedgehog stimulates maturation of Cubitus interruptus into a labile transcriptional activator. *Nature* **396**, 749–753 (1998).
8. J. Jia *et al.*, Shaggy/GSK3 antagonizes Hedgehog signalling by regulating Cubitus interruptus. *Nature* **416**, 548–552 (2002).
9. M. G. Smelkinson, D. Kalderon, Processing of the Drosophila hedgehog signaling effector Ci-155 to the repressor Ci-75 is mediated by direct binding to the SCF component Slimb. *Curr. Biol.* **16**, 110–116 (2006).
10. P. Aza-Blanc, F. A. Ramírez-Weber, M. P. Laget, C. Schwartz, T. B. Kornberg, Proteolysis that is inhibited by hedgehog targets Cubitus interruptus protein to the nucleus and converts it to a repressor. *Cell* **89**, 1043–1053 (1997).
11. Z. Zhang *et al.*, Ter94 ATPase complex targets k11-linked ubiquitinated ci to proteasomes for partial degradation. *Dev. Cell* **25**, 636–644 (2013).
12. W. Zhang *et al.*, Hedgehog-regulated Costal2-kinase complexes control phosphorylation and proteolytic processing of Cubitus interruptus. *Dev. Cell* **8**, 267–278 (2005).
13. D. J. Robbins, D. L. Fei, N. A. Riobo, The Hedgehog signal transduction network. *Sci. Signal* **5**, re6 (2012).
14. Z. Zhou *et al.*, Deubiquitination of Ci/Gli by Usp7/HAUSP regulates Hedgehog signaling. *Dev. Cell* **34**, 58–72 (2015).
15. C. H. Chen *et al.*, Nuclear trafficking of Cubitus interruptus in the transcriptional regulation of Hedgehog target gene expression. *Cell* **98**, 305–316 (1999).
16. T. Von Ohlen, D. Lessing, R. Nusse, J. E. Hooper, Hedgehog signaling regulates transcription through cubitus interruptus, a sequence-specific DNA binding protein. *Proc. Natl. Acad. Sci. U.S.A.* **94**, 2404–2409 (1997).
17. H. Akimaru *et al.*, Drosophila CBP is a co-activator of cubitus interruptus in hedgehog signalling. *Nature* **386**, 735–738 (1997).
18. Y. Han, Q. Shi, J. Jiang, Multisite interaction with Sufu regulates Ci/Gli activity through distinct mechanisms in Hh signal transduction. *Proc. Natl. Acad. Sci. U.S.A.* **112**, 6383–6388 (2015).
19. Y. Han *et al.*, Phosphorylation of Ci/Gli by fused family kinases promotes Hedgehog signaling. *Dev. Cell* **50**, 610–626.e4 (2019).
20. Q. Zhang *et al.*, A hedgehog-induced BTB protein modulates hedgehog signaling by degrading Ci/Gli transcription factor. *Dev. Cell* **10**, 719–729 (2006).
21. J. Bai, Y. Uehara, D. J. Montell, Regulation of invasive cell behavior by taiman, a Drosophila protein related to AIB1, a steroid receptor coactivator amplified in breast cancer. *Cell* **103**, 1047–1058 (2000).
22. J. Lozano, T. Kayukawa, T. Shinoda, X. Belles, A role for Taiman in insect metamorphosis. *PLoS Genet.* **10**, e1004769 (2014).
23. P. K. Byun *et al.*, The Taiman transcriptional coactivator engages toll signals to promote apoptosis and intertissue invasion in Drosophila. *Curr. Biol.* **29**, 2790–2800.e4 (2019).
24. M. Li *et al.*, A steroid receptor coactivator acts as the DNA-binding partner of the methoprene-tolerant protein in regulating juvenile hormone response genes. *Mol. Cell Endocrinol.* **394**, 47–58 (2014).
25. M. Jindra, X. Bellés, T. Shinoda, Molecular basis of juvenile hormone signaling. *Curr. Opin. Insect Sci.* **11**, 39–46 (2015).
26. C. Zhang *et al.*, The ecdysone receptor coactivator Taiman links Yorkie to transcriptional control of germline stem cell factors in somatic tissue. *Dev. Cell* **34**, 168–180 (2015).
27. C. Wang *et al.*, Taiman acts as a coactivator of Yorkie in the Hippo pathway to promote tissue growth and intestinal regeneration. *Cell Discov.* **2**, 16006 (2016).
28. S. Jones, An overview of the basic helix-loop-helix proteins. *Genome Biol.* **5**, 226 (2004).
29. E. Y. Lee *et al.*, Hedgehog pathway-regulated gene networks in cerebellum development and tumorigenesis. *Proc. Natl. Acad. Sci. U.S.A.* **107**, 9736–9741 (2010).
30. B. York, B. W. O'Malley, Steroid receptor coactivator (SRC) family: Masters of systems biology. *J. Biol. Chem.* **285**, 38743–38750 (2010).
31. I. U. Agoulnik *et al.*, Role of SRC-1 in the promotion of prostate cancer cell growth and tumor progression. *Cancer Res.* **65**, 7959–7967 (2005).
32. C. A. Walsh, L. Qin, J. C. Tien, L. S. Young, J. Xu, The function of steroid receptor coactivator-1 in normal tissues and cancer. *Int. J. Biol. Sci.* **8**, 470–485 (2012).
33. L. Li, C. X. Deng, Q. Chen, SRC-3, a steroid receptor coactivator: Implication in cancer. *Int. J. Mol. Sci.* **22**, 4760 (2021).
34. J. Yan, S. Y. Tsai, M. J. Tsai, SRC-3/AIB1: Transcriptional coactivator in oncogenesis. *Acta Pharmacol. Sin.* **27**, 387–394 (2006).
35. K. A. O'Donnell *et al.*, A Sleeping Beauty mutagenesis screen reveals a tumor suppressor role for Ncoa2/Src-2 in liver cancer. *Proc. Natl. Acad. Sci. U.S.A.* **109**, E1377–E1386 (2012).
36. S. Dasgupta *et al.*, Coactivator SRC-2-dependent metabolic reprogramming mediates prostate cancer survival and metastasis. *J. Clin. Invest.* **125**, 1174–1188 (2015).
37. D. Maier, S. Cheng, D. Faubert, D. R. Hipfner, A broadly conserved g-protein-coupled receptor kinase phosphorylation mechanism controls Drosophila smoothened activity. *PLoS Genet.* **10**, e1004399 (2014).
38. Y. Chen *et al.*, G protein-coupled receptor kinase 2 promotes high-level Hedgehog signaling by regulating the active state of Smo through kinase-dependent and kinase-independent mechanisms in Drosophila. *Genes. Dev.* **24**, 2054–2067 (2010).
39. S. Peyrefitte, D. Kahn, M. Haenlin, New members of the Drosophila Myc transcription factor subfamily revealed by a genome-wide examination for basic helix-loop-helix genes. *Mech. Dev.* **104**, 99–104 (2001).
40. R. Burke *et al.*, Dispatched, a novel sterol-sensing domain protein dedicated to the release of cholesterol-modified hedgehog from signaling cells. *Cell* **99**, 803–815 (1999).
41. Y. Ding *et al.*, Hippo signaling suppresses tumor cell metastasis via a Yki-Src42A positive feedback loop. *Cell Death Dis.* **12**, 1126 (2021).
42. C. Molnar, H. Holguin, F. Mayor Jr., A. Ruiz-Gomez, J. F. de Celis, The G protein-coupled receptor regulatory kinase GPRK2 participates in Hedgehog signaling in Drosophila. *Proc. Natl. Acad. Sci. U.S.A.* **104**, 7963–7968 (2007).
43. J. Jia, C. Tong, B. Wang, L. Luo, J. Jiang, Hedgehog signalling activity of Smoothened requires phosphorylation by protein kinase A and casein kinase I. *Nature* **432**, 1045–1050 (2004).
44. J. P. Charles *et al.*, Ligand-binding properties of a juvenile hormone receptor, Methoprene-tolerant. *Proc. Natl. Acad. Sci. U.S.A.* **108**, 21128–21133 (2011).
45. Y. X. Li *et al.*, Juvenile hormone induces methoprene-tolerant 1 phosphorylation to increase interaction with Taiman in Helicoverpa armigera. *Insect Biochem. Mol. Biol.* **130**, 103519 (2021).
46. M. J. Plevin, M. M. Mills, M. Ikura, The LxxLL motif: A multifunctional binding sequence in transcriptional regulation. *Trends Biochem. Sci.* **30**, 66–69 (2005).

47. C. Liu *et al.*, Hedgehog signaling downregulates suppressor of fused through the HIB/SPOP–Crn axis in Drosophila. *Cell Res.* **24**, 595–609 (2014).
48. S. K. Ogden, M. Ascano Jr., M. A. Stegman, D. J. Robbins, Regulation of Hedgehog signaling: A complex story. *Biochem. Pharmacol.* **67**, 805–814 (2004).
49. Z. Yuan *et al.*, Frequent requirement of hedgehog signaling in non-small cell lung carcinoma. *Oncogene* **26**, 1046–1055 (2007).
50. N. Méthot, K. Basler, Suppressor of fused opposes hedgehog signal transduction by impeding nuclear accumulation of the activator form of Cubitus interruptus. *Development* **127**, 4001–4010 (2000).
51. Q. Shi, Y. Han, J. Jiang, Suppressor of fused impedes Ci/Gli nuclear import by opposing Trn/Kapβ2 in Hedgehog signaling. *J. Cell Sci.* **127**, 1092–1103 (2014).
52. K. S. Ho, K. Suyama, M. Fish, M. P. Scott, Differential regulation of Hedgehog target gene transcription by Costal2 and Suppressor of Fused. *Development* **132**, 1401–1412 (2005).
53. G. Wang, K. Amanai, B. Wang, J. Jiang, Interactions with Costal2 and suppressor of fused regulate nuclear translocation and activity of cubitus interruptus. *Genes Dev.* **14**, 2893–2905 (2000).
54. Q. T. Wang, R. A. Holmgren, The subcellular localization and activity of Drosophila cubitus interruptus are regulated at multiple levels. *Development* **126**, 5097–5106 (1999).
55. D. Kent, E. W. Bush, J. E. Hooper, Roadkill attenuates Hedgehog responses through degradation of Cubitus interruptus. *Development* **133**, 2001–2010 (2006).
56. M. Li, E. A. Mead, J. Zhu, Heterodimer of two bHLH-PAS proteins mediates juvenile hormone-induced gene expression. *Proc. Natl. Acad. Sci. U.S.A.* **108**, 638–643 (2011).
57. Z. Zhang, J. Xu, Z. Sheng, Y. Sui, S. R. Palli, Steroid receptor co-activator is required for juvenile hormone signal transduction through a bHLH-PAS transcription factor, methoprene tolerant. *J. Biol. Chem.* **286**, 8437–8447 (2011).
58. M. McIlroy *et al.*, Interaction of developmental transcription factor HOXC11 with steroid receptor coactivator SRC-1 mediates resistance to endocrine therapy in breast cancer [corrected]. *Cancer Res.* **70**, 1585–1594 (2010).
59. L. Qin, Z. Liu, H. Chen, J. Xu, The steroid receptor coactivator-1 regulates twist expression and promotes breast cancer metastasis. *Cancer Res.* **69**, 3819–3827 (2009).
60. A. L. Browne *et al.*, Network analysis of SRC-1 reveals a novel transcription factor hub which regulates endocrine resistant breast cancer. *Oncogene* **37**, 2008–2021 (2018).
61. M. C. Louie, J. X. Zou, A. Rabinovich, H. W. Chen, ACTR/AIB1 functions as an E2F1 coactivator to promote breast cancer cell proliferation and antiestrogen resistance. *Mol. Cell Biol.* **24**, 5157–5171 (2004).
62. S. Dasgupta *et al.*, Metabolic enzyme PFKFB4 activates transcriptional coactivator SRC-3 to drive breast cancer. *Nature* **556**, 249–254 (2018).
63. A. Arimura, M. Peer, A. J. Schröder, P. B. Rothman, The transcriptional co-activator p/CIP (NCoA-3) is up-regulated by STAT6 and serves as a positive regulator of transcriptional activation by STAT6. *J. Biol. Chem.* **279**, 31105–31112 (2004).
64. J. Yan *et al.*, Steroid receptor coactivator-3 and activator protein-1 coordinately regulate the transcription of components of the insulin-like growth factor/AKT signaling pathway. *Cancer Res.* **66**, 11039–11046 (2006).
65. S. Suresh *et al.*, SRC-2-mediated coactivation of anti-tumorigenic target genes suppresses MYC-induced liver cancer. *PLoS Genet.* **13**, e1006650 (2017).
66. Y. Kim *et al.*, Selective down-regulation of glioma-associated oncogene 2 inhibits the proliferation of hepatocellular carcinoma cells. *Cancer Res.* **67**, 3583–3593 (2007).
67. X. Sun *et al.*, Usp7 regulates Hippo pathway through deubiquitinating the transcriptional coactivator Yorkie. *Nat. Commun.* **10**, 411 (2019).
68. Y. Li *et al.*, Dual functions of Rack1 in regulating Hedgehog pathway. *Cell Death Differ.* **27**, 3082–3096 (2020).
69. Z. Zhou *et al.*, Stability of HIB-Cul3 E3 ligase adaptor HIB is regulated by self-degradation and availability of its substrates. *Sci. Rep.* **5**, 12709 (2015).
70. A. Yang *et al.*, Exploiting spatiotemporal regulation of FZD5 during neural patterning for efficient ventral midbrain specification. *Development* **151**, dev202545 (2024).
71. W. Wang *et al.*, Exosomes secreted by palmitic acid-treated hepatocytes promote LX-2 cell activation by transferring miRNA-107. *Cell Death Discov.* **7**, 174 (2021).
72. H. Sasaki, C. Hui, M. Nakafuku, H. Kondoh, A binding site for Gli proteins is essential for HNF-3beta floor plate enhancer activity in transgenics and can respond to Shh in vitro. *Development* **124**, 1313–1322 (1997).
73. M. Cai *et al.*, Nuclear receptor coactivator 2 promotes human breast cancer cell growth by positively regulating the MAPK/ERK pathway. *Front. Oncol.* **9**, 164 (2019).